STUDY ON LUBRICATION CHARACTERISTICS OF HIGH-SPEED ANGULAR CONTACT BALL BEARINGS UNDER TWO-PHASE FLOW

Xinhua GAO [1], Jiahao WANG [2], Qiang BIAN[3], Xinghong WANG [4], Chunjiang ZHAO [5, *]

This study develops a comprehensive two-phase flow computational model incorporating the Volume of Fluid method and Multiple Reference Frame approach, specifically accounting for oil-air flow characteristics. Systematic analysis of lubrication behavior elucidates the distribution patterns and governing mechanisms of lubricant deposition on ball surface under varying operational conditions. Key findings indicate an inverse relationship between bearing rotational speed and lubricant retention in the fluid domain of the ball, while nozzle angle, lubricant viscosity, and air supply pressure exhibit non-monotonic influences on lubricant volume, each displaying distinct optimal values. These results provide fundamental insights for lubrication parameter optimization in high-speed bearing systems.

Keywords: Angular contact ball bearings; Oil-air lubrication; Oil-air two-phase flow; Lubrication; Viscosity

1. Introduction

Rolling bearings constitute critical mechanical components widely employed in high-precision and heavy-duty rotating machinery [1-3], whose operational performance and durability are fundamentally determined by lubrication characteristics. Inadequate lubrication represents a predominant cause of premature bearing failure [4,5], driving the increasing adoption of oil-air lubrication as the preferred solution for high-speed rolling bearing applications [6-8]. This technological advancement necessitates systematic investigation of oil-air

* Corresponding author
[1] School of Mechanical Engineering , Taiyuan University of Science and Technology, Taiyuan 030024, China, e-mail: S202312210066@stu.tyust.edu.cn
[2] School of Mechanical Engineering , Taiyuan University of Science and Technology, Taiyuan 030024, China, e-mail: S202412210177@stu.tyust.edu.cn
[3] School of Mechanical Engineering , Taiyuan University of Science and Technology, Taiyuan 030024, China, e-mail: B202112310026@stu.tyust.edu.cn
[4] School of Mechanical Engineering , Taiyuan University of Science and Technology, Taiyuan 030024, China, e-mail: S202212210261@stu.tyust.edu.cn
[5,*] Prof., School of Mechanical Engineering, Taiyuan University of Science and Technology, Taiyuan 030024, China, e-mail: zhaochj75@163.com

lubrication mechanisms under diverse operating conditions to enable optimal bearing design, enhanced performance, and extended service life.

The nozzle in oil-air lubrication systems critically affects internal lubrication characteristics. Researchers have optimized nozzle designs to enhance lubrication efficiency [9,10]. Hongbin Liu et al. identified optimal lubrication positions and nozzle diameters through simulations and experiments [11]. Wei Wu et al. found that multi-nozzle oil supply methods outperform single-nozzle methods in specific speed ranges [12]. Ke Yan et al. examined the impact of the number of nozzles and sealing structures, demonstrating that double-nozzle designs with sealing structures help reduce pressure and enhance lubrication [13]. Jing Hu et al. designed a cycloidal nozzle structure, reducing lubricant consumption by 20% compared to traditional designs [14]. Xintian Zi et al. developed a guided structure nozzle and conducted experimental comparisons with traditional designs, finding that the guided nozzle consumed less oil [15]. Gloeckner et al. examined the lubrication efficiency. They used the outer ring injection method in their analysis. Their findings showed a substantial decrease in lubricating oil consumption [16]. These studies primarily focused on nozzle structure and distribution. However, due to the complex operating conditions of bearings, further research is needed to explore lubrication characteristics under multiple coupled conditions to develop precise strategies.

Some important progress has also been made in the study of air flow mechanism and lubricating oil distribution in bearing cavity. Kim et al. found that as speed increases, air flow forms high-speed vortices around the balls, hindering effective oil entry into contact areas [17]. Adeniyi et al. developed a numerical computational model of rolling bearings using ANSYS. Their model revealed the relationship between lubricant distribution within the bearing cavity and bearing speed, taking into account both the revolution and rotation of the balls [18]. Bei Yan et al. investigated different oil supply methods and their effects on air flow patterns and lubrication performance, detailing the movement and spread of oil droplets within the bearing cavity [19]. Qunfeng Zeng et al. demonstrated that low-viscosity PAO6 oil optimizes annular flow at the oil-air inlet [20]. Baogang Wen et al. conducted simulations and experiments to analyze the characteristics of lubricant distribution under different nozzle positions. The results revealed that the nozzle position is closely associated with the distribution of lubricant within the bearing cavity [21]. Yang Li et al. utilized CFD(Computational Fluid Dynamics) simulations to create an oil-air lubrication model, showing inlet velocity's effect on flow uniformity [22].

Existing research mainly focuses on the optimization of nozzle construction and the flow characteristics, while lacking studies on local lubrication characteristics. Therefore, this paper takes the 7005C bearing as the subject of investigation. To simulate the revolution and rotation of the balls during bearing

operation, the MRF(Multiple Reference Frame) model is utilized. The VOF(Volume of Fluid) method, which is employed to monitor the oil-air flow, thereby analyzing the distribution of lubricant on the ball surface during stable bearing operation. Additionally, the effects and mechanisms of rotational speed, air supply pressure, nozzle angle, and lubricating oil viscosity are investigated. The findings offer theoretical support for exploring oil-air lubrication mechanisms in high-speed angular contact ball bearings.

2. Mathematical models

This study utilized the VOF model to simulate the internal flow field of oil-air lubrication in bearings, aiming to precisely analyze the two-phase flow process. Under normal operating conditions, the bearing cavity contains both oil and air. By solving single momentum equation, the VOF model can simulate multiple immiscible fluids. Within the domain, it also tracks the volume fraction of each fluid.

To better describe the operating state of the bearing, the MRF method was employed to simulate both revolution and rotation. The rotating fluid domain rotates around the rotating coordinate system at an angular velocity, and the movement of any point can be described as:

$$v = v_r + u_r \tag{1}$$

$$u_r = v_t + \omega \times r \tag{2}$$

Where r represents the displacement vector from the rotational axis to the fluid domain; v_t represents the velocity due to coordinate system rotation; u_r represents the transport velocity; v_r represents the speed relative to the fixed coordinate system; and v represents the absolute velocity.

The RNG k-ε turbulence model, which accounts for high curvature, high strain rates, and other effects, was used to enhance the calculation accuracy under turbulent conditions.

During operation, the outer ring stays fixed in position, while the inner ring rotates around its axis. Assuming there is no relative sliding between the ball and both the outer and inner rings, the revolution and rotation speeds of the balls are given by:

$$n_m = n_i(1-\lambda) \tag{3}$$

$$n_b = \frac{(n_i - n_m)d_m(1-\lambda)}{D} \tag{4}$$

$$\lambda = \frac{D\cos\alpha}{d_m} \tag{5}$$

Where α represents the bearing contact angle; D represents the ball diameter; d_m represents the pitch diameter; n_b represents the rotation speed of the ball; n_i

represents the speed of bearing inner ring; n_m represents the revolution speed of ball. Figure 1 is the schematic diagram of bearing motion.

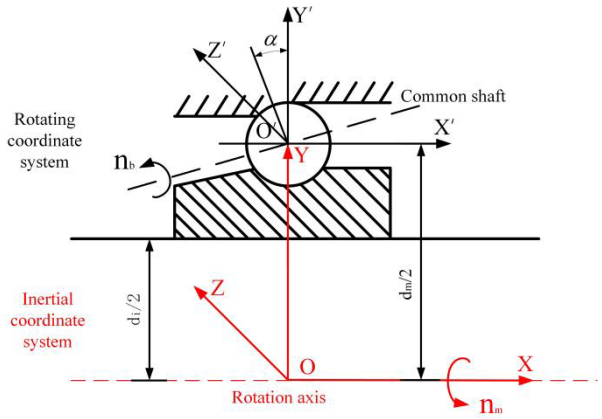

Fig. 1. Motion diagram of the bearing

3. Computational modeling

3.1 Model setup

A 7005C angular contact ball bearing was established as shown in Figure 2(a). By applying Boolean operations to the bearing's solid domain, its fluid domain is depicted in Figure 2(b), with parameters detailed in Table 1. The nozzles are installed at the lateral position. Select 1/14 of the bearing for modelling. The angles between the nozzle and the XOY plane were 0°, 15°, 20°, and 25°, respectively. The nozzle diameter was 0.7 mm, and the air inlet diameter was 0.6 mm. The entire bearing involves complex geometric structures and boundary conditions, resulting in a significant computational load. To improve computational efficiency and ensure feasibility, the physical model was simplified in this study. Specifically, due to the bearing's flow field distribution is periodic, 1/14 of the bearing was picked out to be the object of study. This simplification significantly reduces the computational load while retaining the key characteristics of internal fluid motion and lubrication behavior. For the contact between the balls and the inner and outer rings as well as the cage, we simplify it by referring to the method in reference [23], maintaining a fixed value of 0.1587mm between the rollers and the inner and outer rings as well as the cage. Moreover, the focus of this study is the lubrication characteristics of the roller ball surface rather than the elastic hydrodynamic lubrication of the bearing. By conducting an in-depth analysis of the localized small model, the lubrication patterns under different operating conditions are revealed, providing a reliable reference for the lubrication design and performance optimization.

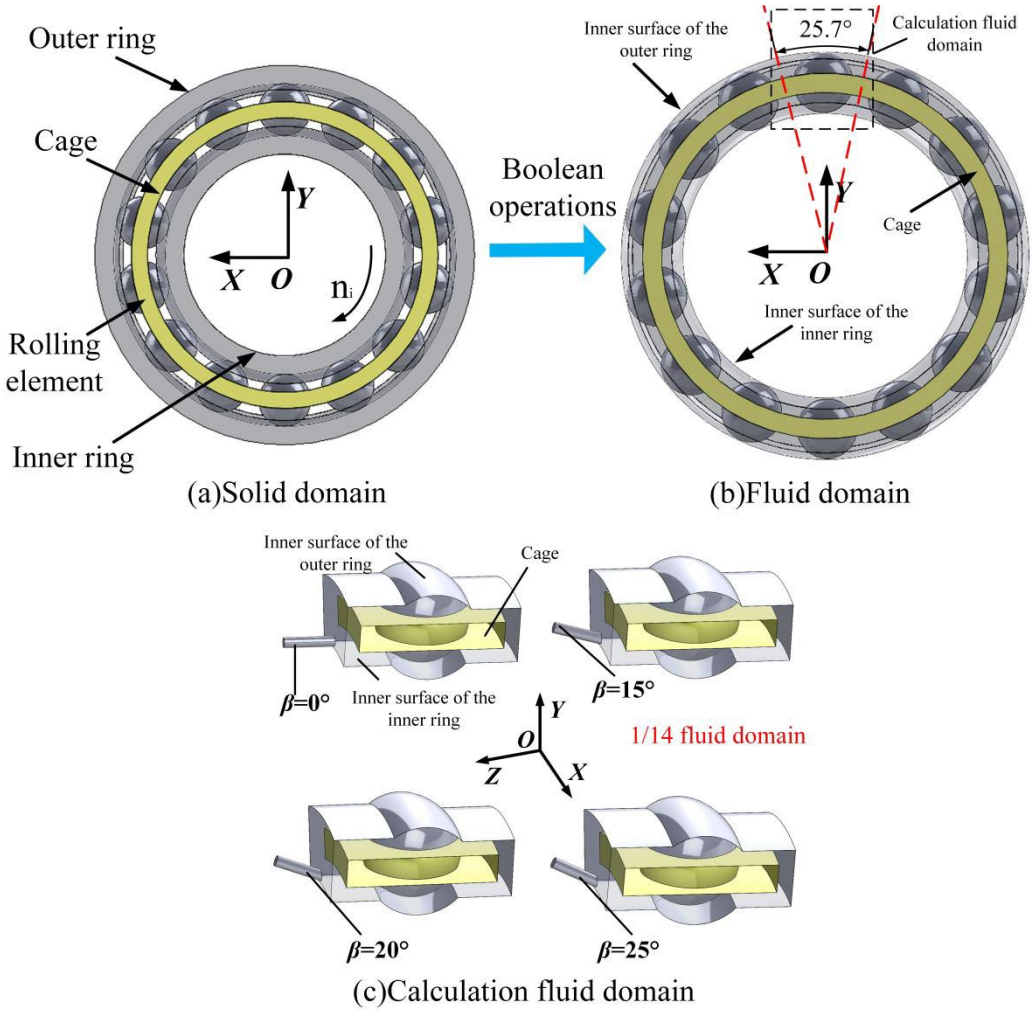

Fig. 2. Physical model

Table 1

Bearing parameters

Parameters	Value
Outer diameter D_o/mm	47
Inner diameter D_i/mm	25
Bearing width B/mm	12
Ball diameter D/mm	6.35
Number of balls N	14
Contact angle α/°	15

Based on the actual running condition, The outer ring serves as a fixed boundary, while the inner ring, cage, and balls function as rotating boundaries. The oil inlet functions as a velocity inlet, the air inlet acts as a pressure inlet, and the outlet is designated as a pressure outlet, working temperature is 293.15K. The mesh is generated using ICEM, with the overall model divided into hexahedral mesh. The

model is divided into three regions to simulate the rotation and revolution of the ball: the domain of the main cavity region, the fluid domain of the ball, and the oil-air inlet, as shown in Figure 3. The revolution speed of the ball defines the velocity in the fluid domain of the ball in the inertial coordinate system. Within the rotating coordinate framework, the self-rotation velocity of the ball defines the boundary condition of the wall. In FLUENT, the region close to the wall is treated with the standard wall function. The momentum equation and turbulence equation both adopt the second-order upwind scheme. The pressure term is discretized using the "PRESTO!" scheme. Finally, the Coupled algorithm is used to solve the discrete algebraic equations. When the residual value is lower than 10^{-4} and the net flux from the inlet to the outlet reaches about 0.5%, it is considered to have converged.

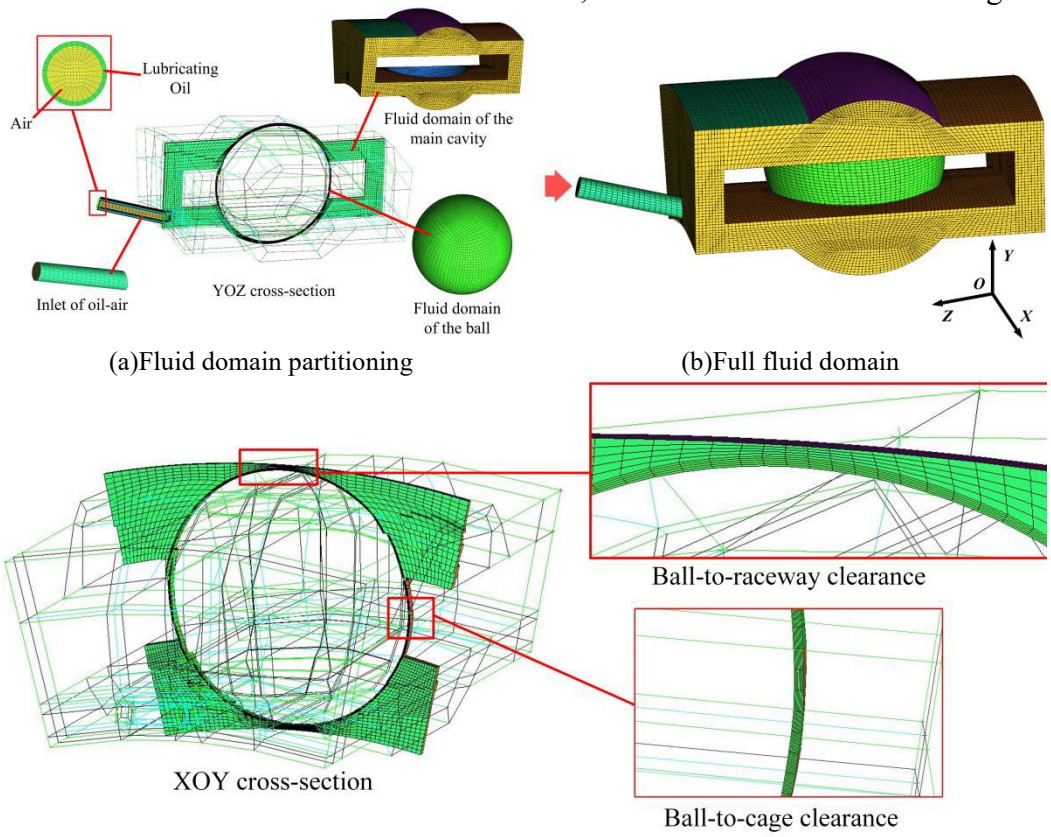

(a)Fluid domain partitioning (b)Full fluid domain

(c)Local mesh refinement

Fig. 3. Mesh model

3.2 Grid independence verification

The operating parameters selected for this study are as follows: rotational speed(n_i)=1.5×10^4 r/min, air supply pressure (P_{in}) = 0.2 MPa, nozzle angle (β) = 15°, and lubricant viscosity (γ) = 30 mm^2/s. Given that the primary lubrication effect originates from the fluid domain of the ball, the oil volume fraction in this region was evaluated across different mesh densities.

To assess mesh sensitivity, the number of nodes was systematically doubled in each iteration, generating four distinct mesh configurations. The corresponding mesh parameters and computational errors are summarized in Table 2. The results indicate that when the mesh density reaches or exceeds 1.6×10^5 nodes, the variation in the oil volume fraction within the fluid domain of the ball remains below 5%. Consequently, the (b) mesh configuration was adopted for subsequent simulations in this study.

Table 2

Mesh parameters and errors

Group	Mesh number	Mesh quality	Oil volume fraction(%)	Error(%)
(a)	81519	0.506707	4.495	——
(b)	163019	0.505732	3.16491	29.59
(c)	327303	0.520258	3.08982	2.37
(d)	622185	0.520258	3.02013	2.25

4. Results and analysis

4.1 Rotational speed

The influence of rotational speed on lubricant distribution characteristics is systematically presented in Figure 4, demonstrating an inverse correlation between rotational speed and both the oil volume fraction in the fluid domain of the ball and the oil spray volume on ball surfaces. To elucidate this phenomenon, we conducted a comprehensive pressure analysis across seven strategically selected cross-sections (Figure 5). The results reveal distinct pressure distribution patterns: peripheral cross-sections exhibit minimal pressure variations (approaching atmospheric conditions) regardless of rotational speed, whereas the central cross-section maintains significantly higher pressure that exhibits positive speed dependence. This behavior can be attributed to intensified shear-driven airflow at elevated rotational speeds. The enhanced shear effects promote lubricant ejection from the bearing cavity, consequently reducing both the retained oil volume fraction and spray deposition.

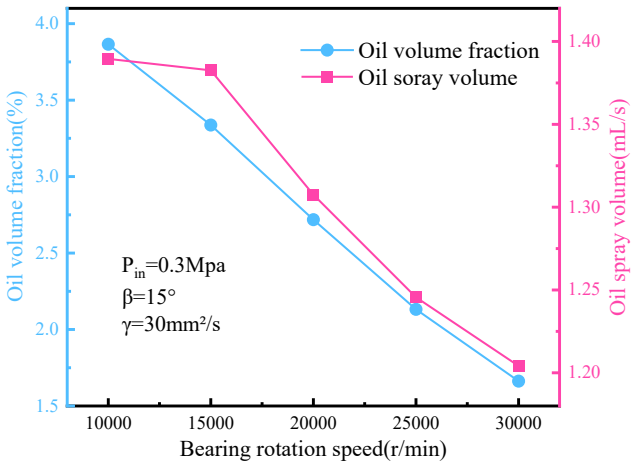

Fig. 4. Effect of speed on volume fraction and spray volume of the oil

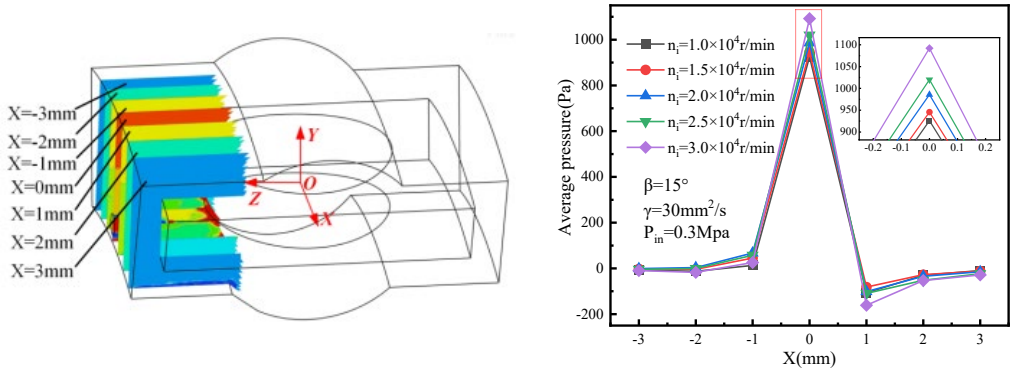

(a)Position of each section (b)Average pressure at each section

Fig. 5. Average pressure of each section at different speeds

4.2 Air supply pressure

Figure 6 demonstrates a non-monotonic relationship between air supply pressure and oil volume fraction in the fluid domain of the ball, exhibiting an initial increase followed by subsequent decrease, with maximum oil retention occurring at 0.3 MPa. Complementary data in Figure 7 reveals a distinct positive correlation between air supply pressure and oil spray volume on the ball surface. This consistent growth trend suggests that elevated air pressures promote more efficient lubricant transport to bearing surfaces.

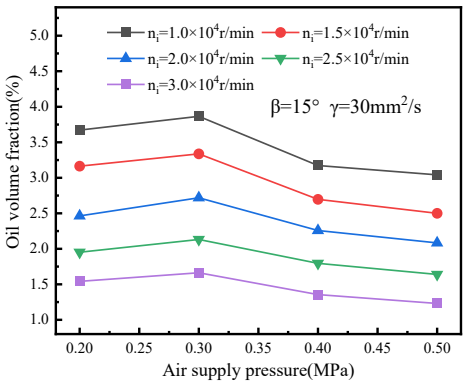

Fig. 6. Effect of air supply pressure on oil volume fraction

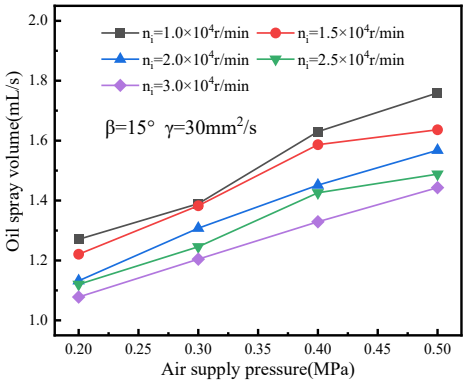

Fig. 7. Effect of air supply pressure on oil spray volume

The underlying mechanism is elucidated in Figure 8, which quantifies the pressure-dependent lubricant injection dynamics. Experimental measurements show that increasing air supply pressure from 0.2 to 0.5 MPa enhances injection velocity by 43.8% (from 9.17 m/s to 13.2 m/s). This accelerated injection velocity directly contributes to improved oil delivery efficiency, explaining the observed increase in surface spray volume.

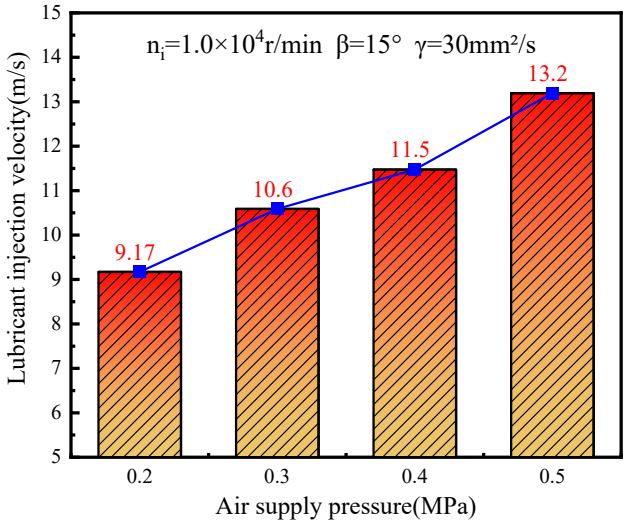

Fig. 8. Effect of air supply pressure on lubricant injection velocity

Figure 9 systematically examines the relationship between air supply pressure and lubrication characteristics through comparative analysis of lubricant streamlines and surface coverage patterns. The results demonstrate a pressure-dependent lubrication mechanism wherein low injection velocities at reduced pressures result in incomplete surface coverage due to insufficient momentum transfer. As pressure increases, enhanced injection velocity promotes more

effective lubricant delivery to the ball surface, achieving optimal wetting conditions. However, beyond a critical pressure threshold, the intensified aerodynamic forces induce significant lubricant ejection from the lubrication zone, creating a distinct peak in oil volume fraction followed by gradual depletion. Notably, while elevated pressures improve distribution uniformity through enhanced flow momentum, this benefit is counterbalanced by reduced lubricant retention efficiency at higher pressure levels, revealing an inherent trade-off in high-pressure lubrication systems.

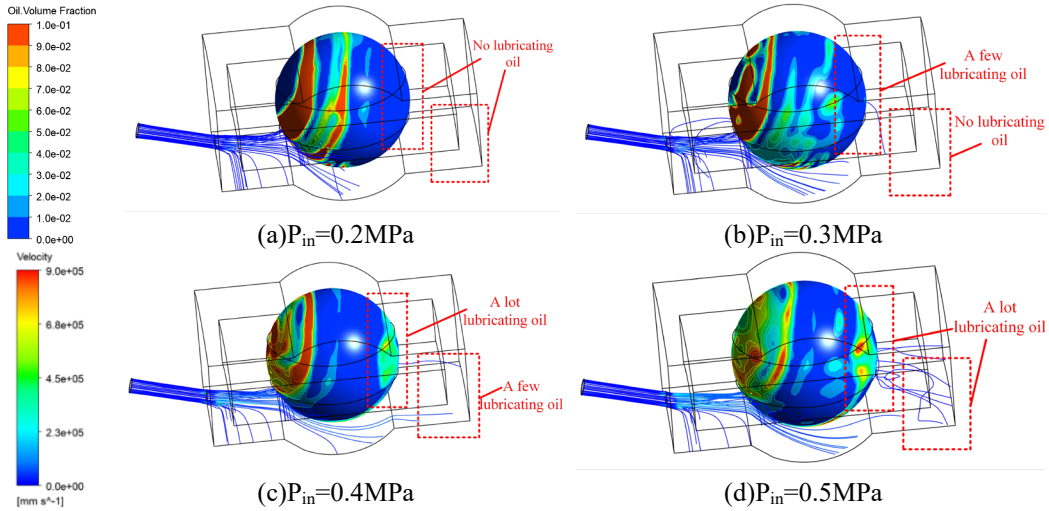

(a)P_{in}=0.2MPa (b)P_{in}=0.3MPa

(c)P_{in}=0.4MPa (d)P_{in}=0.5MPa

Fig. 9. The lubricant streamlines and lubricant film distribution on the ball surface under different air supply pressures, n_i=1.0×10^{4}r/min,β=15°,γ=30mm²/s

4.3 Nozzle angle

Figure 10 and Figure 11 present the systematic investigation of nozzle angle effects on lubrication characteristics, demonstrating a non-monotonic relationship between nozzle angle and both oil volume fraction in the fluid domain of the ball and surface spray volume. The calculation results reveal a distinct peak in lubrication performance at intermediate nozzle angles, with significant variations observed across different operating conditions. Specifically, at 10,000 r/min, the oil volume fraction exhibits a 112.4% differential between 15° and 20° nozzle configurations. This angular dependence becomes less pronounced at higher rotational speeds, as evidenced by the reduced 87.1% variation observed at 30,000 r/min. These findings quantitatively demonstrate that increased rotational speed attenuates the nozzle angle's influence on lubricant distribution, suggesting a competing mechanism between centrifugal and injection momentum effects in the lubrication process.

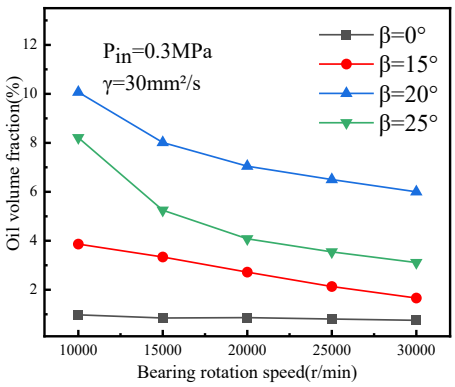

Fig. 10. Oil volume fraction at various nozzle angles

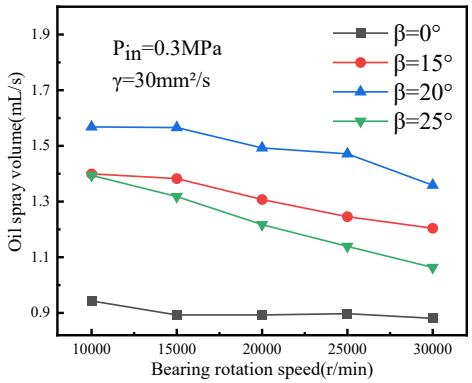

Fig. 11. Oil spray volume at various nozzle angles

Figure 12 illustrates the influence of nozzle angle on lubricant streamlines and lubricant film distribution on the ball surface. When the nozzle is oriented at 0° (directly facing the ball surface), the lubricant exhibits significant dispersion, resulting in unstable oil film formation. Progressive increases in nozzle angle improve lubricant retention on the ball surface, facilitating complete oil film development. When the nozzle angle is 20°, the lubricant achieves maximum coverage and uniform distribution on the ball surface, resulting in optimal lubricant film continuity and the lowest risk of wear. Beyond this critical angle, lubricant trajectory shifts toward the inner ring, leading to reduced ball surface coverage. These results demonstrate that direct nozzle orientation (0°) toward the ball surface should be avoided to ensure effective lubrication.

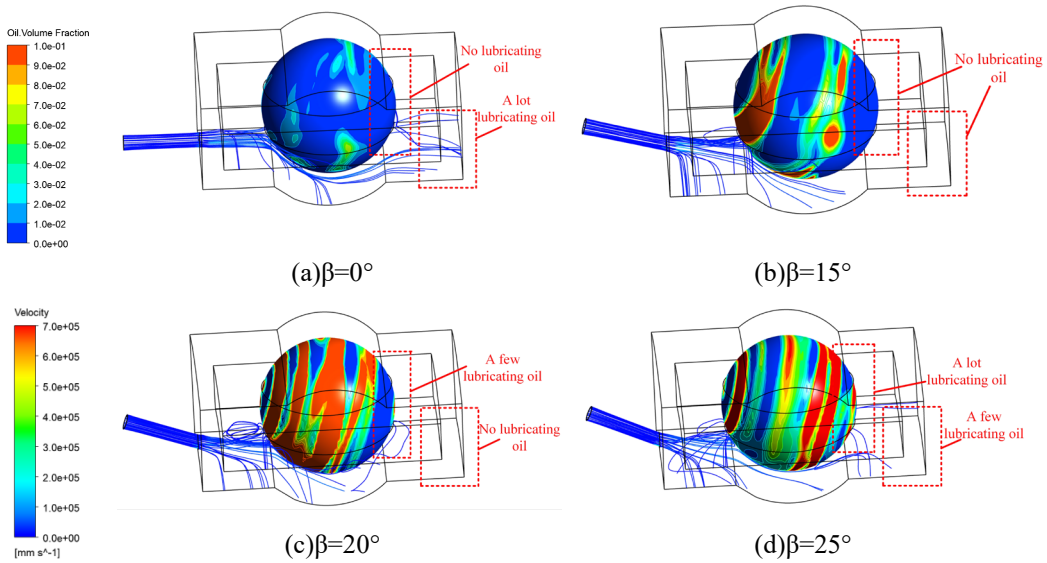

Fig. 12. The lubricant streamlines and lubricant film distribution on the ball surface under different nozzle angles, n_i=1.5×10^{4}r/min,P_{in}=0.3MPa,γ=30mm²/s

4.4 Lubricant viscosity

Lubricant parameters are given in Table 3. By modifying the properties of the lubricant, this study compares the lubrication conditions of the bearing under various lubricant.

Table 3

Lubricant parameters

Lubricant Type	Density ρ/(kg/m^3)	Viscosity mm^2/s
(a)	997	12.4
(b)	970	15.6
(c)	925	19.7
(d)	897	22
(e)	876	30

The viscosity-dependent lubrication characteristics are systematically presented in Figures 13-15. Figure 13 reveals a distinct peak in theoil volume fraction within the fluid domain of the ball at an optimal viscosity of 22 mm²/s, demonstrating a non-monotonic relationship between viscosity and lubricant retention. This behavior is complemented by the viscosity effects on surface lubrication shown in Figure 14, where the oil spray volume exhibits a consistent inverse relationship with viscosity. The underlying mechanism is quantitatively elucidated in Figure 15, showing that increasing viscosity from 12.4 to 30 mm²/s reduces the lubricant injection velocity by 15.7% (from 12.7 m/s to 10.7 m/s) due to enhanced flow resistance. This velocity reduction directly diminishes the oil spray volume deposited on the ball surface, establishing a clear viscosity-performance correlation in the lubrication system.

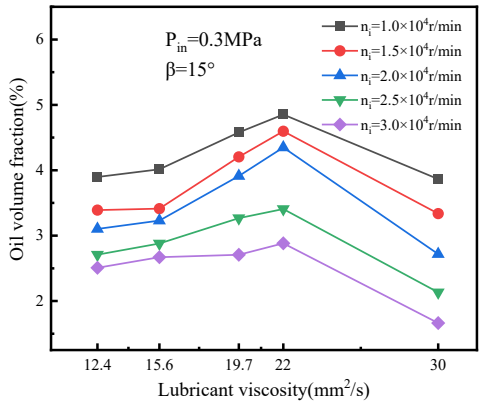

Fig. 13. Oil volume fraction at various lubricant viscosities

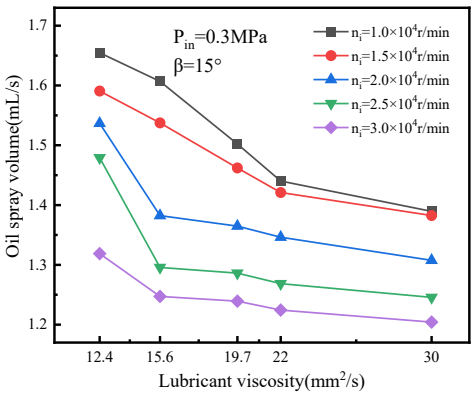

Fig. 14. Oil spray volume at various lubricant viscosities

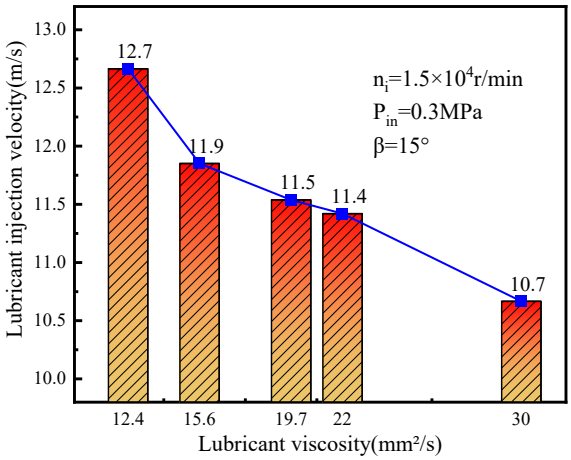

Fig. 15. Lubricant injection velocity under different lubricant viscosities

Figure 16 presents a comparative analysis of lubricant streamlines and lubricant film distribution on the ball surface under varying lubricant viscosities. The results demonstrate a non-monotonic relationship between viscosity and lubrication performance. Lower viscosity conditions exhibit higher injection velocities, yet fail to establish a continuous lubricant film. Conversely, increasing viscosity reduces injection velocity, leading to incomplete surface coverage. Consequently, the oil volume fraction displays a parabolic trend with viscosity, initially increasing before decreasing. Optimal lubrication uniformity is achieved at an intermediate viscosity of 22 mm²/s, where the lubricant distribution across the ball surface reaches maximum homogeneity.

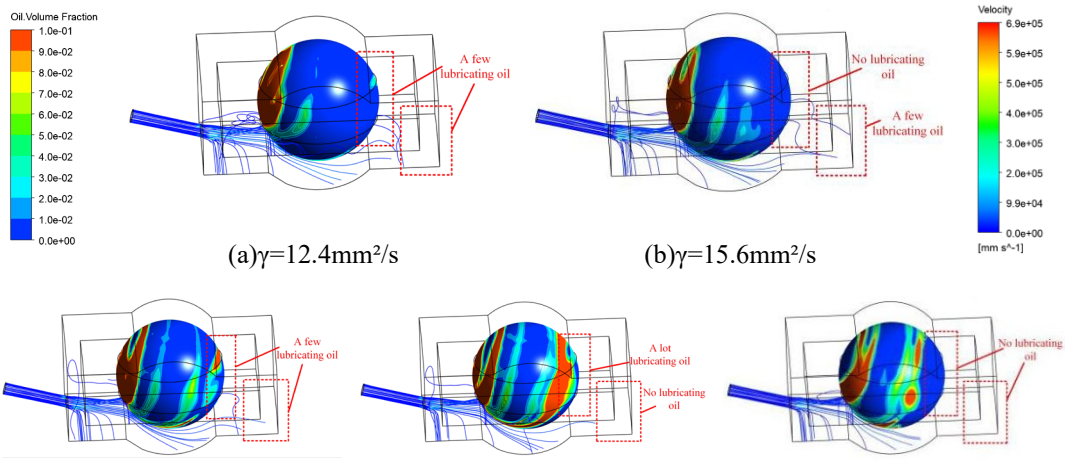

(a)γ=12.4mm²/s (b)γ=15.6mm²/s

(c)γ=19.7mm²/s (d)γ=22mm²/s (e)γ=30mm²/s

Fig. 16. The lubricant streamlines and lubricant film distribution on the ball surface under different lubricant viscosities, n_i=1.0×10⁴r/min,β=15°,P_{in}=0.3MPa

5. Model validation

To validate the accuracy of the constructed model, this study employed the proposed grid generation strategy and model parameter configuration to establish a simulation model based on the geometric characteristics and physical conditions specified in Reference [24], with detailed parameter settings provided in Table 4. Comparative analysis between the simulation results and experimental data from Reference [24] (as illustrated in Figure 17(a)) demonstrated high consistency in both the lubricant distribution patterns and velocity field characteristics. Figure 17(b) presents the influence of bearing rotational speed on the airflow velocity and pressure distributions at the inner contact interface.

The results indicate a significant positive correlation between bearing speed and both airflow velocity and pressure. Specifically, at 70,000 r/min, the maximum error in airflow velocity simulation was controlled within 4.13%, while at 10,000 r/min, the pressure simulation error did not exceed 13.25%. These error margins fall within the acceptable range for engineering applications, thereby substantiating the validity and reliability of the proposed modeling methodology and analytical framework.

Table 4

Verify bearing parameters

Structural Parameter	Value
Outer Diameter Do/mm	55
Inner Diameter Di/mm	30
Bearing Width B/mm	13
Ball Diameter D/mm	6.35
Number of Balls N	17
Contact Angle α/°	15

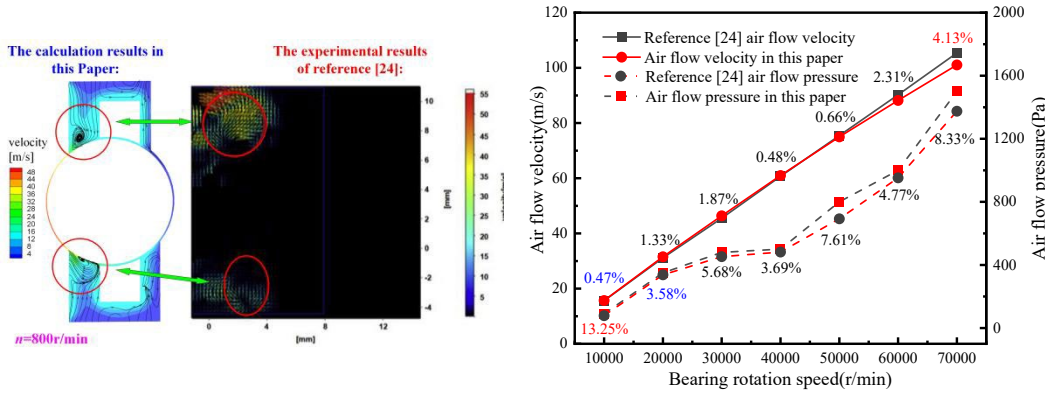

(a) Comparison of experimental results (b) Comparison of calculation results

Fig. 17. Comparison of Results

6. Conclusions

The conclusions derived from the simulations within the parameter ranges of this study are as follows:

(1)Within the speed range of 10,000 r/min to 30,000 r/min, the ball surface's oil volume fraction decreases as the rotational speed rises.

(2)As the air supply pressure increases, the ball surface's oil volume fraction first increases and then decreases. The lubricant distribution on the ball surface becomes more uniform with higher air supply pressure.

(3)In oil-air lubrication, the nozzle should not directly face the ball. As the nozzle angle increases, the ball surface's oil volume fraction first increases and then decreases. The lubrication effect is best at a nozzle angle of 20°, where the lubricant distribution on the ball surface is most uniform.

(4)As the lubricant viscosity increases, the ball surface's oil volume fraction first increases and then decreases. The best lubrication effect occurs at a viscosity of 22 mm²/s, where the lubricant distribution is most uniform.

Acknowledgement

This work was financially supported by the Major scientific and technological projects in Shanxi Province (20201102003), Shanxi coal-based low carbon joint fund (No. U1610118), Graduate Innovation Program of Taiyuan University of Science and Technology(BY2023018).

REFERENCES

[1] *Wang Y, Li S, Wei C,* et al. Study on motorized spindle with full ceramic ball bearings and lubrication at high speeds, Journal of Ceramic Processing Research, **25**(4), 2024, pp. 643-659.

[2] *Liu H, Chen Y, Guo Y,* et al. Coupling study on quasi-static and mixed thermal elastohydrodynamic lubrication behavior of precision high-speed machine spindle bearing with spinning, Machines, **12**(5), 2024, 325.

[3] *Junning L I, Xiaojie T.* Research on Anti-Wear Properties of Nano-Lubricated High-Speed Rolling Bearings under Various Working Conditions, Technical Gazette/Tehnički Vjesnik, **30**(1), 2023.

[4] *Williams T, Ribadeneira X, Billington S,* et al. Rolling element bearing diagnostics in run-to-failure lifetime testing, Mechanical Systems and Signal Processing, **15**(5), 2001, pp. 979-993.

[5] *Winkler A, Bartz M, Wartzack S.* Numerical wear modeling in the mixed and boundary lubrication regime, Lubricants, **10**(12), 2022, 334.

[6] *Su C, Chen W.* Effect of temperature rise on a tandem of ball-bearings with an O-configuration in motorized spindle under oil-air lubrication, Thermal Science and Engineering Progress, **45**, 2023, 102117.

[7] *Dudorov E A, Ruzanov A I, Zhirkin Y V.* Introducing an oil-air lubrication system at a continuous-casting machine, Steel in Translation, **39**(4), 2009, pp. 351-354.

[8] *Zeng Q, Zhang J, Hong J*, et al. A comparative study on simulation and experiment of oil-air lubrication unit for high speed bearing, Industrial Lubrication and Tribology, **68**(3), 2016, pp. 325-335.
[9] *Li S, Guo F, Li X*, et al. Elastohydrodynamic lubrication with oil droplets, Tribology Letters, **65**(4), 2017, 162.
[10] *Li X, Guo F, Wang S*, et al. Behaviors of a micro oil droplet in an EHL contact, Friction, **4**(4), 2013, pp. 359-368.
[11] *Liu H, Li Y and Liu G*. Numerical investigation of oil spray lubrication for transonic bearings, Journal of the Brazilian Society of Mechanical Sciences and Engineering, **40**(8), 2018, 401.
[12] *Wu W, Hu J, Yuan S*, et al. Numerical and experimental investigation of the stratified air-oil flow inside ball bearings, International Journal of Heat and Mass Transfer, **103**, 2016, pp. 619-626.
[13] *Yan K, Wang Y, Zhu Y*, et al. Investigation on the effect of sealing condition on the internal flow pattern of high-speed ball bearing, Tribology International, **105**, 2017, pp. 85-93.
[14] *Hu J, Xun B, Zhang X*, et al. Design and research of new-type nozzle structure based on oil–air lubrication, Meccanica, **59**(1), 2024, pp. 1-18.
[15] *Zi X, Chen K, Bai Q*, et al. The Enhancement of Oil Delivery and Bearing Performance via A Guiding-Structured Nozzle under Oil–Air Lubrication, Lubricants, **12**(2), 2024, 60.
[16] *Gloeckner P, Martin M, Flouros M*. Comparison of power losses and temperatures between an all-Steel and a direct outer ring-cooled, hybrid 133-mm-bore ball bearing at very high speeds, Tribology Transactions, **60**(6), 2017, pp. 1148-1158.
[17] *Oh I S, Kim D, Hong S W*, et al. Three-dimensional air flow patterns within a rotating ball bearing, Advanced Science Letters, **19**(8), 2013, pp. 2180-2183.
[18] *Adeniyi A A, Morvan H P and Simmons K A*. A multiphase computational study of oil-air flow within the bearing sector of aeroengines, American Society of Mechanical Engineers, **56734**, 2015, V05CT15A024.
[19] *Yan B, Dong L, Yan K*, et al. Effects of oil-air lubrication methods on the internal fluid flow and heat dissipation of high-speed ball bearings, Mechanical Systems and Signal Processing, **151**, 2021, 107409.
[20] *Zeng Q, Zhang J, Hong J*, et al. Numerical Investigation on Flow Pattern of Air-Oil with Different Viscosities Lubrication, Engineering, **9**(1), 2017, pp. 1-13.
[21] *Wen B, Li Y, Li Y*, et al. Influence and Optimization of Nozzle Position on Lubricant Distribution in an Angular Contact Ball Bearing Cavity, Lubricants, **12**(12), 2024, 419.
[22] *Li Y, Yang Z, Chen F*, et al. Effect of air inlet flow rate on flow uniformity under oil-air lubrication, Industrial Lubrication and Tribology, **70**(2), 2018, pp. 282-289.
[23] *Peterson W, Russell T, Sadeghi F*, et al. A CFD investigation of lubricant flow in deep groove ball bearings, Tribology International, **154**, 2021, 106735.
[24] *Yan K, Dong L, Zheng J*, et al. Flow performance analysis of different air supply methods for high speed and low friction ball bearing, Tribology International, **121**, 2018, pp. 94-107.